Contrib Mineral Petrol (1994) 117:331–344

Gerhard Vavra

Systematics of internal zircon morphology in major Variscan granitoid types

Received: 25 October 1993 / Accepted: 14 March 1994

Abstract The internal morphologies of zircon crystals from different types of granitoids (alkaline, calcalkaline and anatectic) are revealed by cathodoluminescence imaging and are described in terms of growth rates of the crystal faces relative to each other. Zircons in the alkaline granitoids are characterized by high and constant growth rates of {010} relative to the pyramidal forms and by symmetric growth of {011}. Zircons in the calcalkaline and anatectic granitoids are characterized by fluctuating or gradually decreasing relative growth rates of {010}, by asymmetric and highly variable growth of {011}, and by a tendency of {110} to become growth-inhibited. Corrosion events are interspersed during zircon growth in the calcalkaline magmas. In the calcalkaline and anatectic magmas, a discontinuity breaks the morphological evolution at late stages of crystallization. The discontinuity coincides with a sharp drop in cathodoluminescence. The growth behaviour of each crystal form is analysed and compared with predictions made by the periodic bond chain (PBC) theory. It is argued that the relative growth rate of {010} depends on supersaturation, that the growth rates of {011} faces are changed in response to different ratios of adsorbing cations (Na, K, Al), and that {110} faces become growth-inhibited by the adsorption of H_2O or trace elements enriched in the residual liquid. Morphological and chemical discontinuities at late stages of crystallization are reasonably explained by the formation of larger growth units (from smaller ionic entities) in the residual liquid. Important factors controlling the zircon morphology in different types of granitoids are: high cooling rates (alkaline magmas), magma mixing (calcalkaline magmas), enrichment of H_2O and trace elements in residual liquids (calcalkaline and anatectic magmas), and the major element chemistry of the magma, possibly the ratio of Na and K to Al (agpaicity).

G. Vavra
Institut für Kristallographie und Petrographie,
Eidgenössische Technische Hochschule Zürich,
Sonneggstrasse 5, CH-8092 Zürich, Switzerland

Editorial responsibility: V. Trommsdorff

Introduction

Minerals are known to develop a variety of crystal shapes in response to their growth environment (Sunagawa 1984). Several approaches have been taken to assess the environmental factors controlling the shape and to use crystal shape as a petrogenetic indicator. The experimental approach (e. g. Caruba 1978; Caruba et al. 1988) is difficult to apply to most natural growth environments. The alternative approach is empirical. It establishes relationships between the crystal shape of minerals and the geological context of rock samples (Sunagawa 1987).

The igneous mineral best studied by the empirical approach is zircon (Speer 1982). This is due to the strong resistance of its morphology to processes in the earth's crust. Previous morphogenetic studies of zircon, since Poldervaart (1956), relied on aspects of the external crystal shape. Pupin and Turco (1972) introduced the typology diagram arranging zircon crystals according to the proportions of the main crystal forms. In several empirical studies (Pupin and Turco 1975; Pupin 1980; Pupin and Turco 1981), a systematic variation of zircon morphology in the major petrogenetic types of granitic rocks was established. Alumina-rich and autochthonous (anatectic) magmas develop {110} and {121},whereas alkaline magmas emplaced at shallow crustal levels develop {010} and {011} as dominant crystal forms. Zircons from calcalkaline magmas were found to have intermediate characteristics.

Since only the external crystal shape was accessible, the dynamic aspect of evolving morphology was largely neglected or was not considered in terms of crystal growth. The morphology was thought to be static by Poldervaart (1956). This concept was revised by several observations (Veniale et al. 1968; Karner and Helgesen 1970; Köhler 1970) showing that zircon morphology

changes during the later stages of magma differentiation. Pupin (1980) derived morphological evolutions from a statistical evaluation of external crystal shapes. He understood the evolution as a sequence of morphological types and maintained that each type forms in response to the chemistry (ratio of alkalies to alumina) and temperature of the magma. It must be critically remarked that zircon typology is an artificial classification of crystal shapes and is not suitable for genetic studies of evolving morphologies. After the imaging of internal zircon morphology was introduced (Vavra 1990; Paterson et al. 1992), it is possible to study zircon morphology in terms of crystal growth.

Extending previous empirical work on the external morphology (Pupin 1980), the present study establishes systematic variations in the growth rates of crystal faces. Variations are expected during crystal growth in a single evolving magma, on the one hand, and between crystals from different types of granitic magmas, on the other hand. From the empirical relationships alone, it is not possible to constrain the physical and chemical factors controlling the growth rates. Therefore, the theoretical growth rates of crystal faces and their responses to environmental conditions as predicted from crystal growth theory (Woensdregt 1992) are compared with the observations. Observations and theory will provide the basis for discussing the aspects of alkaline, calcalkaline and anatectic magma genesis recorded in the internal morphology of zircon.

Methods

Since crystal growth in nature is not accessible to direct observation, the information on growth rates of crystal faces has to be inferred from the internal morphology (growth banding, sector zoning) revealed in crystal sections (Sunagawa 1987). For zircon, the internal morphology is best revealed by cathodoluminescence imaging (Vavra 1990). This has been carried out using a SEM-based cathodoluminescence detection system, at the ETH Zürich. Since the euhedral crystals orient themselves with the largest face parallel to the mounting glass, the internal morphology is imaged on sections parallel to the dominant prism face of crystals. The different growth sectors can be identified by characteristic angles between growth bands (Fig. 1) and the relative growth rates of the crystal faces can be determined. The details of growth behaviour of crystal faces is best presented by sections of individual crystals. In addition, the evaluation of a large data set is required to show that observations on individual crystals are representative for the zircon population in a rock sample. Data of relative growth rates between faces are collected from many crystals and plotted against the distance of the (011) face from the crystal centre, according to the method presented by Vavra (1993). Relative growth rates are plotted for a total of 800 growth increments distributed over 8 granitoid samples. Depending on the variability of relative growth rates, the number of measured growth increments per crystal ranges between 1 and 6.

Characterization of selected granitoid types

The zircons of the present study crystallized in different types of granitoids within the European Variscides. They represent alkaline, calcalkaline, and autochthonous (anatectic) granitic rocks.

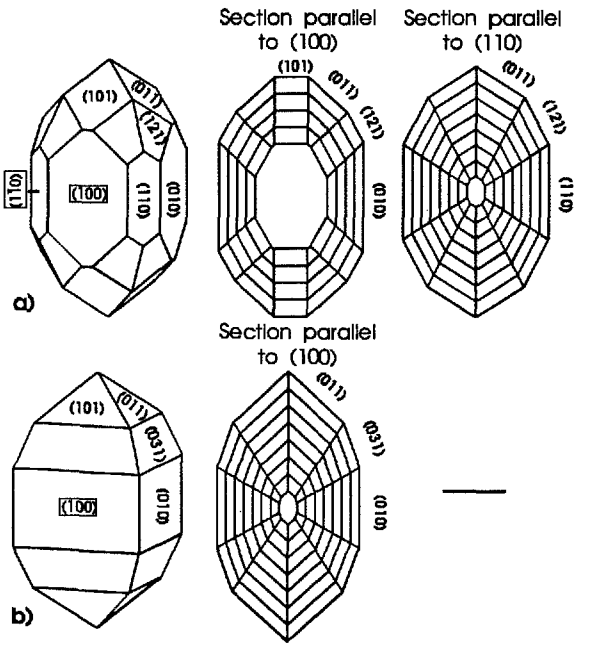

Fig. 1a,b Orientation of crystal sections and growth bands. **a** Calcalkaline and anatectic granitoids. **b** Alkaline granitoids

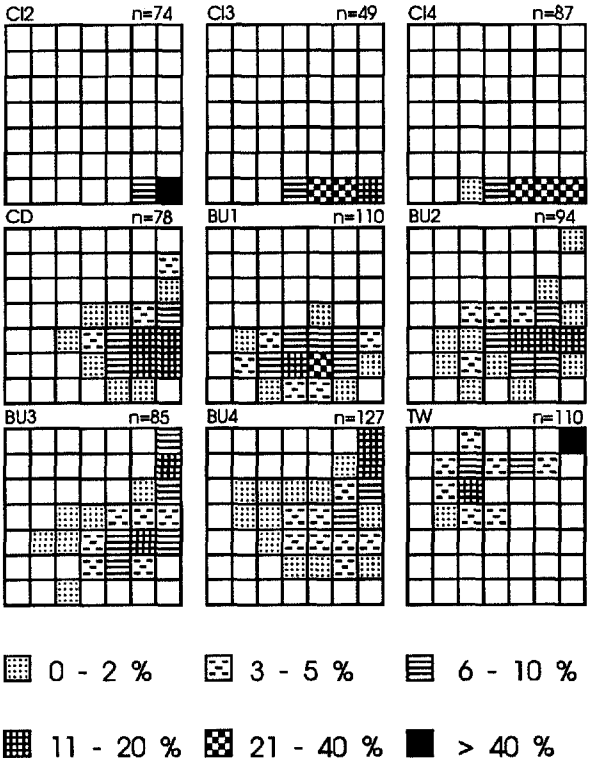

Fig. 2 Frequency distribution of zircon morphology in the typological grid (Pupin 1980) for samples of the present study. *CI*, alkaline granitoids of the Monte Cinto ring complex; *CD*, high-K calcalkaline granodiorite of Cima d'Asta; *BU*, calcalkaline granitoids of the zoned pluton of Budduso; *TW*, autochthonous (anatectic) granodiorite of the Tauern window

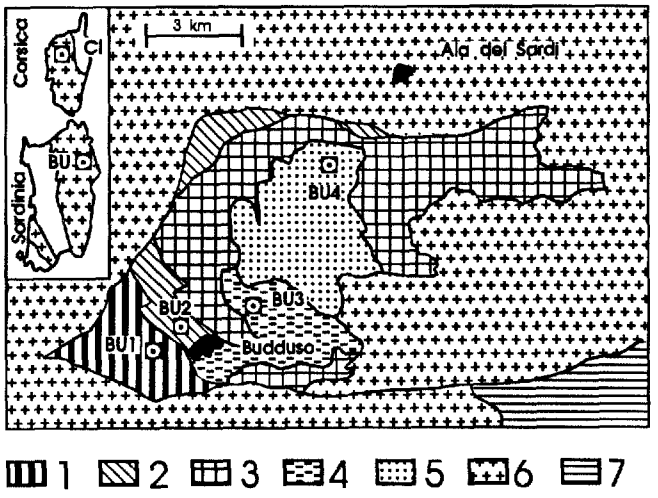

Fig. 3 Concentrically zoned calcalkaline pluton of Budduso with location of samples *BU*1 to *BU*4 (modified after Zorpi et al. 1989). 1, tonalite and 9 ranodiorite; 2, amphibole-bearing monzogranite; 3, biotite-rich monzogranitc; 4, coarse-grained leucogranite; 5, medium-grained leucogranite; 6, other Carboniferous granitoids; 7, metamorphic rocks. Inset, location of calcalkaline Budduso pluton (*BU*) and alkaline ring complex of Monte Cinto (*CI*)

The frequency distributions of external zircon morphology in the typological diagram (Fig. 2) agree with the empirical relationships between morphology and granitoid type as established by Pupin (1980). Some petrographic and geochemical characteristics of the samples and their geological context are briefly described. More detailed information is given in the literature cited.

Alkaline granitoids of the Monte Cinto ring complex (Corsica)

Alkaline granitoids were sampled from the subvolcanic ring complex of Monte Cinto in northern Corsica (Fig. 3 inset; Bonin 1977; Bonin et al. 1987). The samples comprise two granites (CI1 and CI2) from the subvolcanic intrusion of Bonifatu (Bonin 1988), one rhyolite (CI3) from a dyke within the Caldera, and one alkali-feldspar-phyric microgranite (CI4) from a ring dyke outside the eastern Caldera border. The characteristic texture of the samples is a granophyric intergrowth of mesoperthitic feldspar and quartz resulting from cotectic crystallization at hypersolvus (low P_{H2O}) conditions (Shelley 1993, p. 143). Hydrous minerals are absent from the original parageneses. The chemical analyses (Table 1) show the low Al-content, high ratio of Na and K to Al (agpaicity index), and high contents of Y, Zr and Nb typical for alkaline granitoids. The depletion of compatible elements (Sr and Ba) points to differentiation of the magma by fractional crystallization. Bonin et al. (1978) derived a mantle or lowermost crustal origin of a nearby alkaline granite from a low Sr-initial ratio. The Upper Permian and Lower Triassic alkaline magmatism is related to a distensive tectonic regime following the Variscan orogeny (Bonin et al. 1987).

High-K calcalkaline granodiorite of the Atesina-Cima d'Asta volcano-plutonic complex (southern Alps)

The sample was taken from the Cima d'Asta pluton located at the southern margin of the Atesina volcanic complex, in the southern Alps (Barth et al. 1993). It has a high-K calcalkaline chemistry with high contents of K, Rb, Y and Nb (Table 1). The study of mineral equilibria yielded a pressure estimate of less than 0.5 kbar and H_2O-undersaturated conditions at the emplacement of the magma (d'Amico and Franceschini 1985). The granodiorite is associated with cogenetic volcanic rocks. According to its age (275 Ma; Barth et al. 1994), it belongs to the youngest calcalkaline magmatism of the Variscan orogen and is considered to be transitional to the post-orogenic alkaline magmatism (Bonin 1988). Nd isotopic data point to a lower crustal origin (Barth et al. 1993).

Calcalkaline granitoids of the Budduso pluton (Sardinian batholith)

Four samples (BU1 to BU4) are located along a profile from the centre to the rim of the concentrically zoned pluton of Budduso (Bruneton and Orsini 1977; Zorpi et al. 1989) within the Sardinian batholith (Fig. 3). Al-contents are high and the agpaicity indices are low (Table 1). The high contents of Sr and Ba show that differentiation by fractional crystallization was not as important as in the alkaline granitoids. The origin of zoning from the leucogranitic centre to the tonalitic rim is known to be magma mixing (Cocirta et al. 1989), which is documented by mafic autoliths and incomplete equilibration of minerals. The absence of contact metamorphic effects and of cogenetic volcanic rocks points to an

Table 1 X-ray fluorescence analyses. CI, alkaline granitoids from the Monte Cinto ring complex; CD, high-K calcalkaline granodiorite from the Cima d'Asta pluton; BU, calcalkaline granitoids from the zoned pluton of Budduso; TW, anatectic granodiorite from the Tauern Window. L.O.I., loss on ignition. Agp, (Na + K)/Al (agpaicity index). Analysed by Geochemisches Zentrallabor, University of Tübingen

	CI1	CI2	CI3	CI4	CD	BU1	BU2	BU3	BU4	TW
SiO_2	76.74	77.92	78.12	70.96	66.62	66.09	71.76	75.34	74.93	68.37
TiO_2	0.13	0.11	0.14	0.33	0.52	0.52	0.31	0.12	0.09	0.41
Al_2O_3	11.60	11.03	11.03	13.99	16.45	16.06	14.10	13.32	13.32	15.38
Fe_2O_3	2.10	1.80	2.63	3.45	4.19	4.54	3.18	1.83	1.53	3.87
MnO	<0.01	0.05	0.02	0.08	0.06	0.07	0.05	0.03	0.04	0.06
MgO	0.56	<0.23	0.37	<0.23	1.54	1.19	0.64	<0.23	<0.23	1.28
CaO	<0.19	0.50	<0.19	0.40	3.22	4.00	2.50	1.53	1.17	2.68
Na_2O	3.33	3.22	3.95	4.52	3.44	3.53	3.14	2.85	3.10	3.97
K_2O	4.54	4.16	3.60	5.41	3.42	2.79	3.68	4.89	5.02	3.24
P_2O_5	0.18	<0.02	0.17	0.23	0.16	0.30	0.24	0.03	0.02	0.17
L.O.I.	0.46	0.68	0.01	0.27	0.37	0.51	0.30	–0.30	–0.09	1.65
Rb	249	198	166	112	148	54	107	132	150	132
Sr	<14	<14	<14	27	216	217	144	62	66	518
Ba	<45	<45	<45	310	605	880	792	262	236	944
Y	133	110	82	54	35	26	18	20	12	39
Zr	623	400	507	726	200	218	166	102	88	179
Nb	56	44	34	25	19	13	13	9	<7	19
V	<6	<6	<6	<6	54	56	30	10	<6	45
Agp	0.90	0.89	0.94	0.95	0.57	0.55	0.65	0.75	0.79	0.65

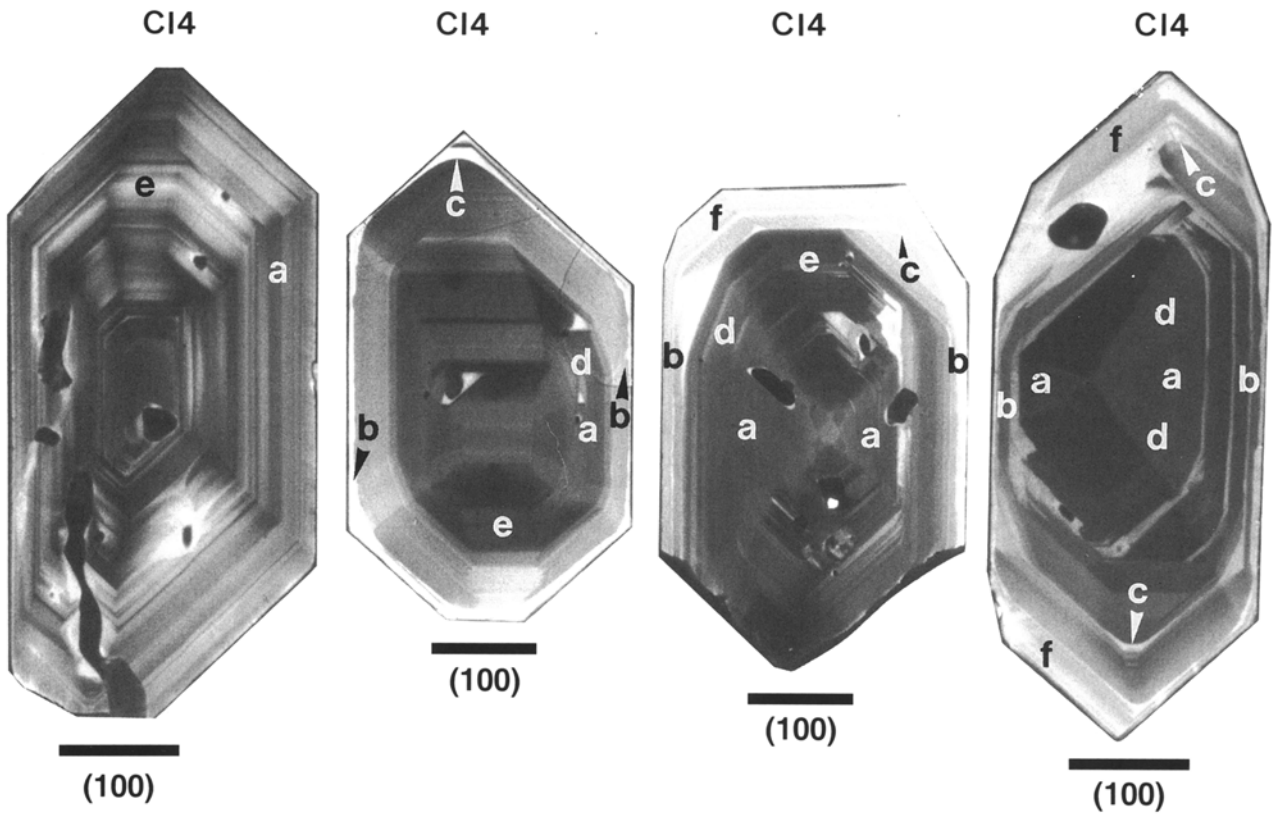
CI4
e
a
(100)
CI4
c
d
b
a
b
e
(100)
CI4
f
e
c
b
d
b
a
a
(100)
CI4
f
c
d
b
a
a
b
b
d
c
f
(100)

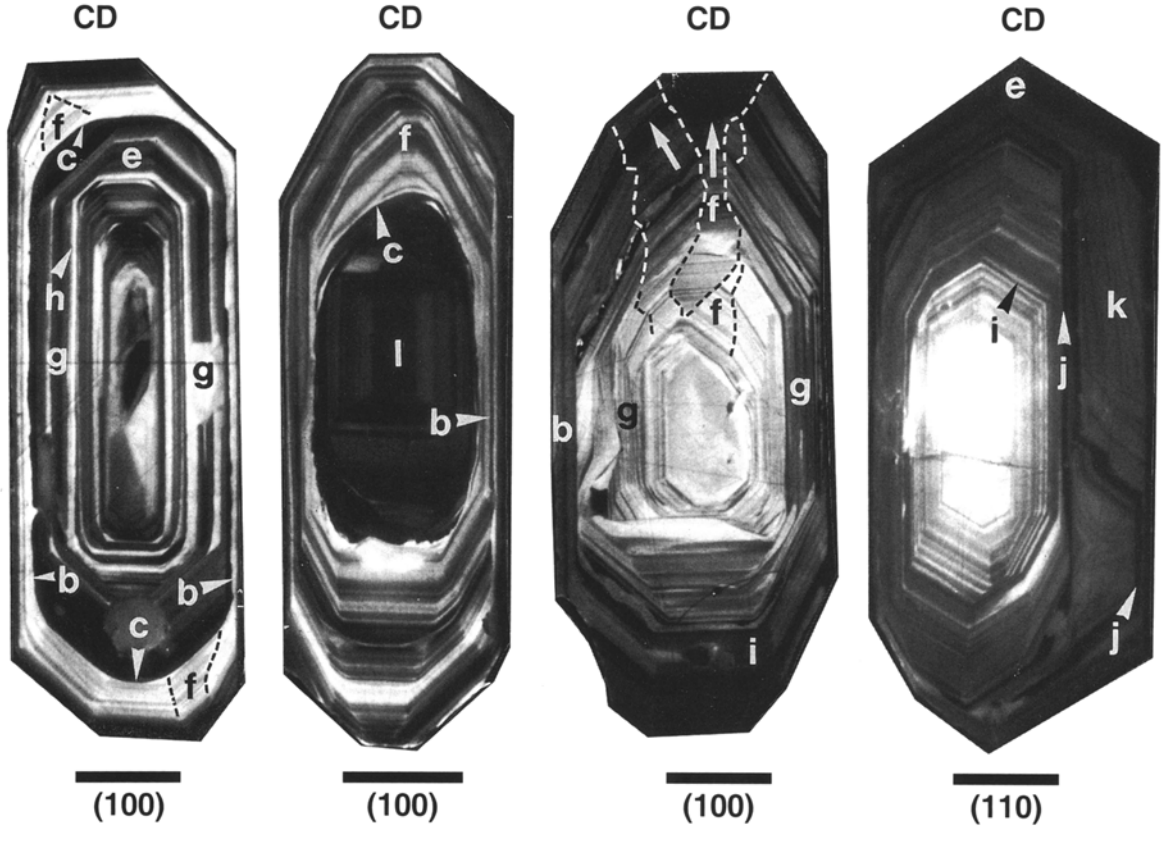
CD
f
c
e
h
g
g
b
b
c
f
(100)
CD
f
c
l
b
(100)
CD
f
f
g
b
g
i
(100)
CD
e
i
k
j
j
(110)

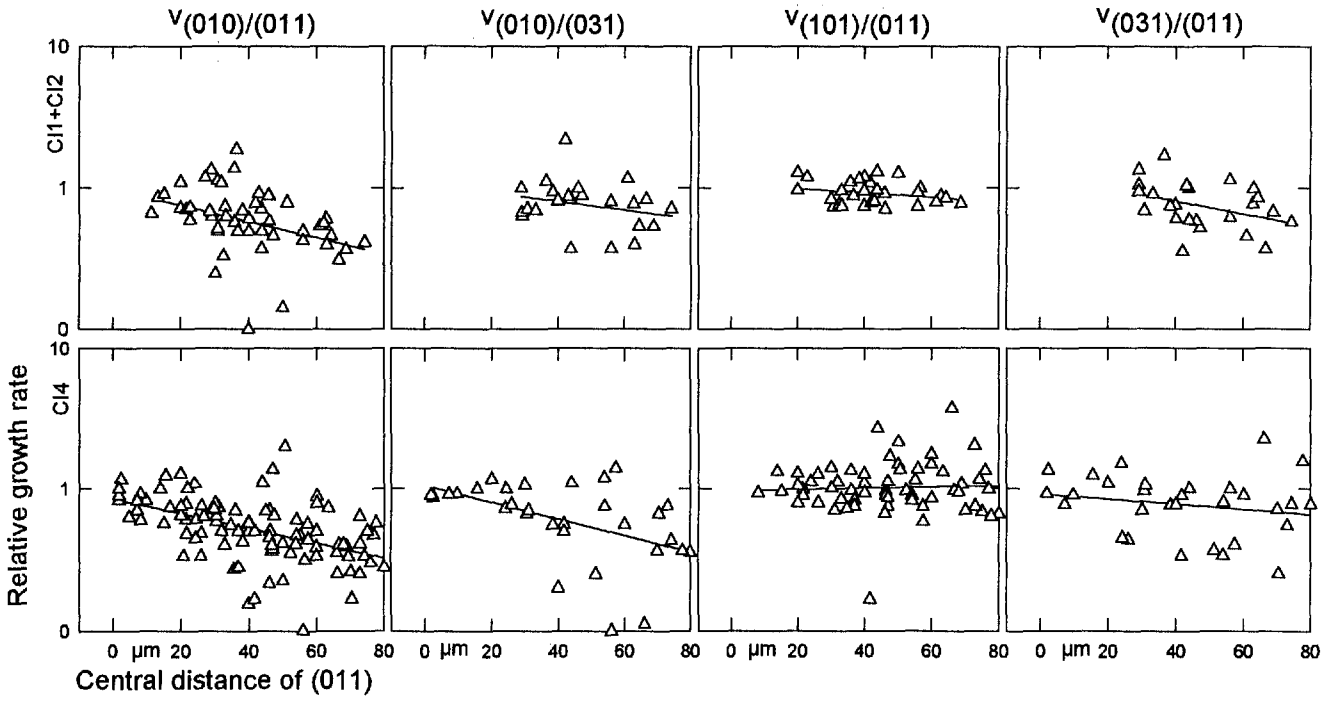

Fig. 5 Diagrams showing relative growth rates of zircon crystal faces versus the central distance of (011) for granitoids of the Monte Cinto alkaline ring complex. Row headings, sample numbers. Column headings, relative growth rates. First-order regression lines are drawn

emplacement level deeper than that of the previously described samples. The age, between 285 and 290 Ma (Vavra and Oberli unpublished U/Pb zircon data), corresponds to the post-collisional stage of the Variscan orogeny.

Autochthonous granodiorite of the Tauern Window (Eastern Alps)

The granodiorite was taken from the Variscan basement in the Tauern Window, specifically from the southern part of the Hochalm massif (Finger and Steyrer 1988; Finger et al. 1993). In this area, migmatitic transitions between the granodiorite and partly anatectic gneisses are observed (Vavra 1989; Holub and Marschallinger 1989). The congruence of trace element patterns (Vavra 1989) supports the origin of the magma by anatectic melting of the quartzo-feldspathic country rocks and its emplacement close to the place of origin. The calcalkaline chemistry was inherited from the molten volcano-detrital sequences (Frisch et al. 1993). Biotite is the only mafic mineral, even in the associated tonalitic rocks of this massif, indicating that H_2O was present in large amounts, at the time of anatexis. The Hochalm granitoids were formed at 315 Ma (Cliff 1981), in a collisional tectonic setting (Vavra and Hansen 1991).

Fig. 4 Cathodoluminescence images of zircon sections. *CI4*, from alkaline granitoids of the Monte Cinto ring complex, *CD*, from high-K calcalkaline granodiorite of Cima d'Asta. *a*, rapid growth of {010} relative to pyramidal faces; *b*, strongly reduced growth rate of {010}; *c*, stages of crystal corrosion overgrown by brightly luminescent bands; *d*, presence of {031} during rapid growth of {010}; *e*, symmetric growth of {011}; *f*, asymmetric growth of {011} (the typical irregular shape of sector boundaries is marked by *dashed lines*); *g*, irregularly fluctuating growth rate of {010}; *h*, intercalated brightly luminescent growth bands; *i*, continuous transition to low-luminescent outer growth zone; *j*, growth inhibition of (110); *k*, resumption of rapid growth on (110) by curved growth bands; *l*, possible inherited core. *Scale bars* 30 µm. The indices below denote the section planes

Observations on internal zircon morphology

Alkaline granitoids of the Monte Cinto ring complex

In the internal parts of all crystals (Fig. 4, CI4 a), the {010} prism grew nearly as fast as the pyramidal faces, giving rise to stubby and even equant crystal habits. In the outer zones of most crystals, where stages of crystal corrosion are interspersed, a strong reduction of the relative growth rate of {010} is observed (Fig. 4, CI4 b, c). The statistical diagrams (Fig. 5) underline the general decrease of relative growth rate of {010}. Since growth increments from many crystals are plotted together, the diagrams do not reveal the detail that the growth rate of {010} decreased sharply, in the outer growth zones.

The {011} pyramidal form grew symmetrically, in the internal growth zones, but changed to asymmetric growth, in the outer growth zones (Fig. 4, CI4 f). This was accomplished by increasing growth rates of some random faces of the form. The asymmetric growth was enhanced after stages of corrosion. The presence of the steep pyramid {031} of zircon (Fig. 4, CI4 d) is a characteristic of the alkaline granitoids. Its average growth rate was slightly less than that of {011} (Fig. 5).

Systematic differences of the morphological evolution between the four samples are not observed. The internal morphology of zircon in the alkaline granitoids is schematically shown in Fig. 6.

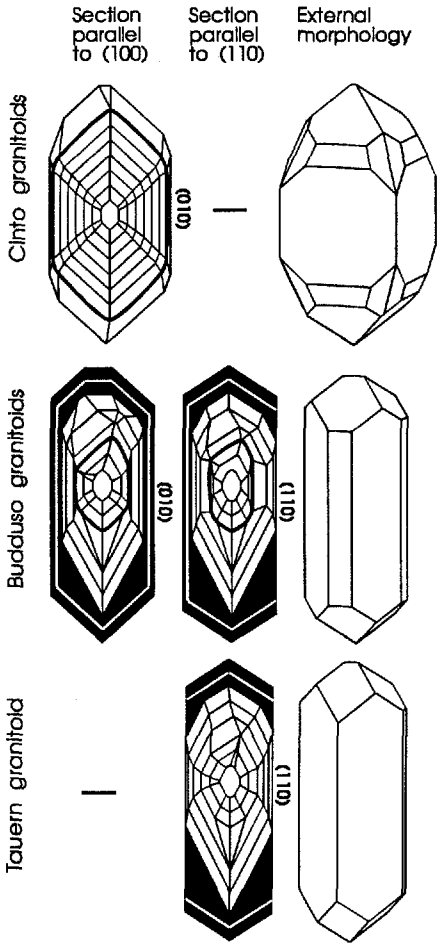

Fig. 6 Generalized schemes of internal and external zircon morphologies in the investigated granitoids. Sections show growth bands and sector boundaries. *Heavy rounded lines* indicate stages of intermittent corrosion. *Black growth bands* indicate distinct low-luminescent overgrowths

High-K calcalkaline granodiorite of the Atesina-Cima d'Asta volcano-plutonic complex

The growth rate of {010} relative to {011} and {121} fluctuated unsystematically and does not show any tendency (Fig. 7, CD). The crystal sections show frequent intercalations of brightly luminescent growth bands (Fig. 4, CD h). Some of them have grown on rounded morphologies after crystal corrosion (Fig. 4, CD c).

Asymmetric growth of {011} occurred frequently and was not confined to the outer growth zones. Due to increased growth rates of random {011} faces, adjacent {121} faces increased in size (Fig. 4, CD f). The steep pyramid {121} itself grew symmetrically, with an average rate slightly lower than that of {011} (Fig. 7, CD).

The {110} prism remained subordinate in most crystals. Only in the outer growth zones of a minor subpopulation, {110} became the dominant prism form. The transition from a dominant {010} to a dominant {110} prism is rather sharp and accomplished by a rapid reduction of the growth rate of {110} faces (Fig. 4, CD j). Some inhibited {110} faces suddenly resumed rapid growth (Fig. 4, CD k) and were again growth-inhibited, at later stages.

Calcalkaline granitoids of the Budduso pluton

In the peripheral tonalite of the zoned pluton (Fig. 3, BU1), the growth rate of {010} relative to {011} and {121} fluctuated without any tendency (Fig. 7, BU1). The lowest relative growth rates of {010} are observed in association with interspersed corrosion events (Fig. 8, BU1 a, b). In the more acidic lithologies towards the centre of the pluton (Fig. 3, BU2 to BU4), a systematic reduction of the {010} growth rate becomes prominent (Fig. 7, BU2 to BU4). The sector boundaries between {010} – and adjacent {121} faces are smoothly curved and tend to become parallel with the *c* axis (Fig. 8, BU3 and BU4 e). In these samples, intermittent stages of zircon corrosion are rare.

The {011} pyramid is characterized by asymmetric growth, in the whole pluton. The asymmetric growth caused the irregular shapes of sector boundaries between {011} and {121} faces, which are partly marked by dashed lines in Fig. 8. Adjacent to fast growing {011} faces, the faces of the steep pyramid {121} increased in size (Fig. 8c). In addition to growing asymmetrically, the {011} faces were the most variable in growth rate. This is shown by the correlated relative growth rates of {121} and {010} faces, both normalized to {011} (Fig. 9). In some crystals, {011} faces increased their growth rates discontinuously to such an extent that they disappeared between the converging sector boundaries of {121} (Fig. 8, BU4 d). The steep pyramid {121} grew symmetrically, with an average growth rate slightly less than that of {011} (Fig. 7).

The {110} prism remained subordinate to {010}, in the samples BU1 and BU2 of the peripheral pluton. In the samples BU3 and, especially in BU4, the growth rate of {110} faces strongly decreased at the outer zones of most crystals (Fig. 8, BU3 and BU4 g). The growth inhibition of {110} faces resulted in increasing elongation of crystals. Some growth-inhibited {110} faces resumed rapid growth after the crystal edges were rounded by minor corrosion (Fig. 8, BU3 h).

A very distinctive morphological evolution started at the latest growth stage of some crystals in samples BU3 and BU4 (rarely also in samples BU1 and BU2). Several crystal forms underwent simultaneous and discontinuous changes in relative growth rates. At the same growth stage, the cathodoluminescence intensity drops sharply (Fig. 8, BU3 and BU4 f). The pyramidal forms are the most strongly affected. The growth of {011} became symmetrical (Fig. 8, BU3 and BU4 j) and its average growth rate decreased relative to {010} (Fig. 7, BU3 and BU4). The growth rate of the steep pyramid {121} was discontinuously increased relative to both {011} and {010} (Fig. 7, BU3 and BU4; Fig. 9), causing its rapid disappearance from the crystal morphology

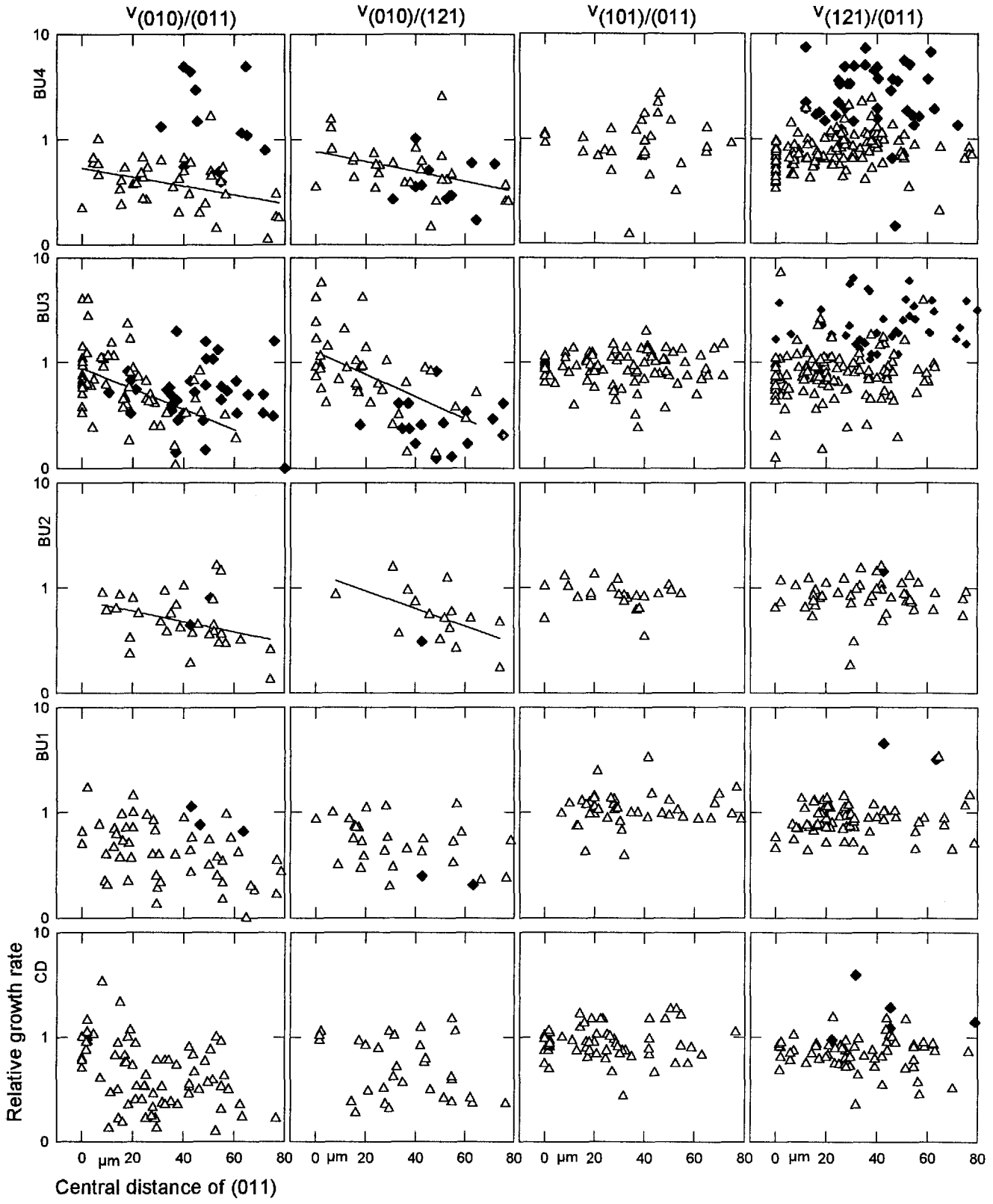

Fig. 7 Diagrams showing relative growth rates of zircon crystal faces versus the central distance of (011) for the high-K calcalkaline granodiorite of the Cima d'Asta pluton (*CD*) and for calcalkaline granitoids of the zoned Budduso pluton (*BU*1-*BU*4). Row headings, sample numbers. Column headings, relative growth rates. *Triangles*, growth increments in high-luminescent zones. *Diamonds*, growth increments in distinct outer low-luminescent zones. Regression lines are drawn where trends are observed

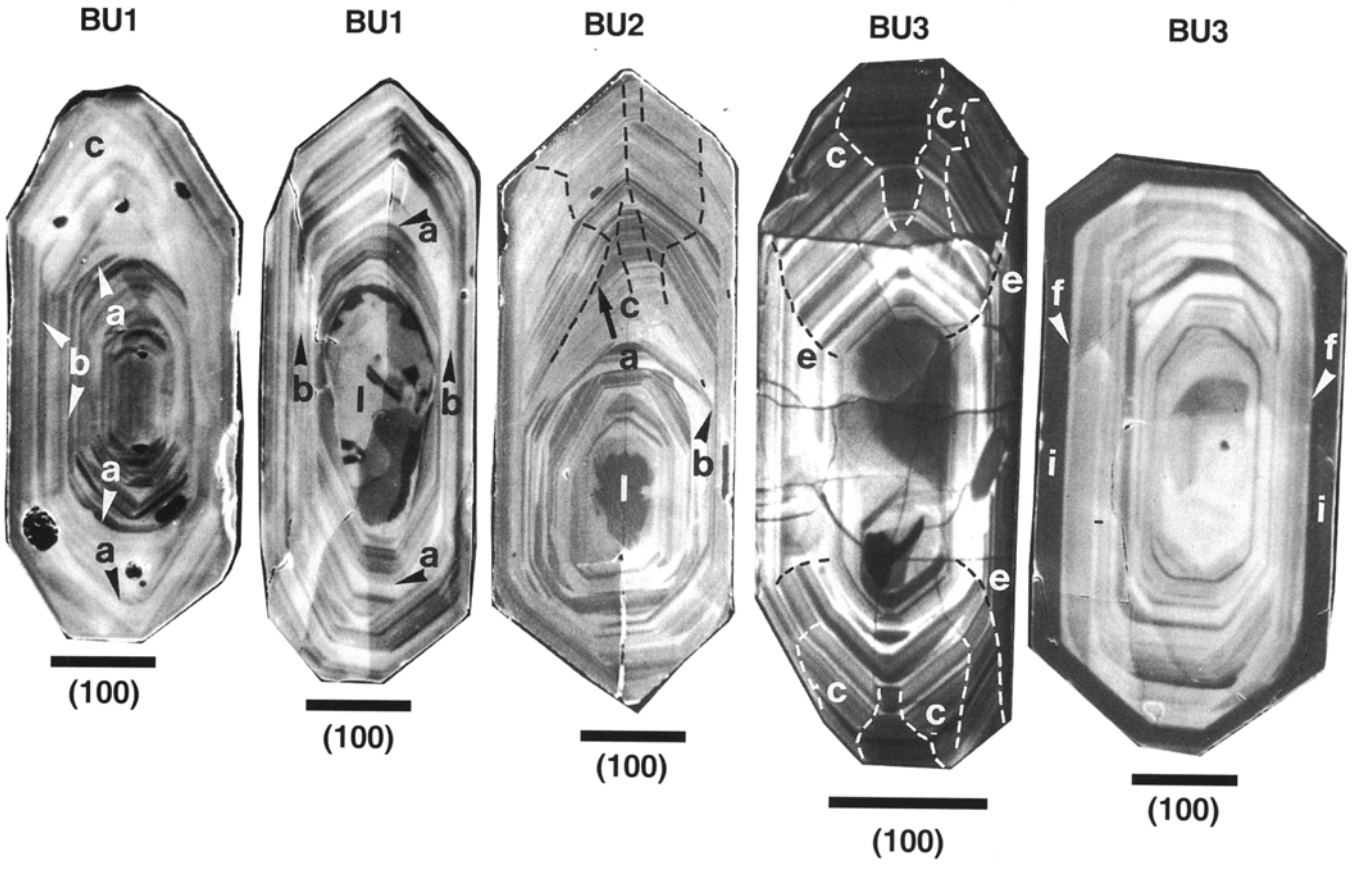
BU1
BU1
BU2
BU3
BU3
(100)
(100)
(100)
(100)
(100)

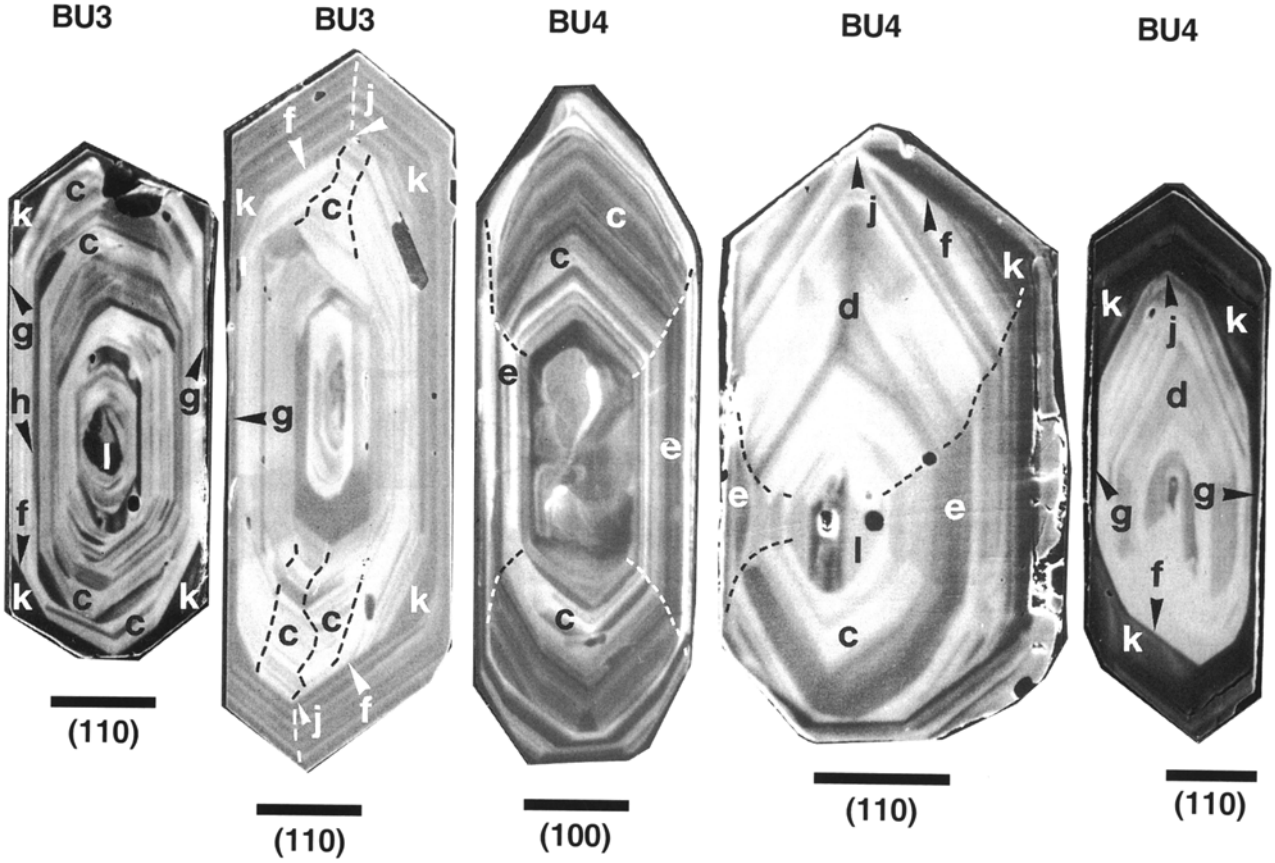
BU3
BU3
BU4
BU4
BU4
(110)
(110)
(100)
(110)
(110)

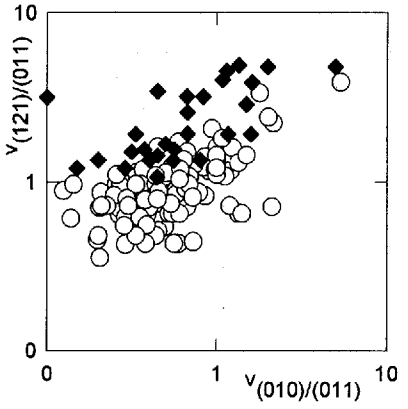

Fig. 9 Correlation between (011)-normalized growth rates for zircon crystal faces in the calcalkaline pluton of Budduso. *Circles*, growth increments in high-luminescent zones. *Diamonds*, growth increments in distinct outer low-luminescent zones

(Fig. 8, BU3 and BU4 k). The growth rate of {110} became strongly reduced already in the more internal growth zones, but its growth inhibition frequently coincides with the sharp transition to the outer low-luminescent zone (Fig. 8, BU3 and BU4 g). In contrast, the growth of {010} does not appear to be affected at all (Fig. 8, BU3 i).

The characteristics of the internal and the finally resulting external zircon morphology in the central Budduso pluton (BU3 and BU4) are summarized in the schemes of Fig. 6. The external morphology dominated by {110} and {011} mainly resulted from the described discontinuity of relative growth rates at the start of the outer low-luminescent zone.

Autochthonous granodiorite of the Tauern Window

The morphological evolution of zircon in this rock closely resembles that in sample BU4. Only the differences are pointed out. The reduction of the growth rate of {110} faces at outer growth zones and their final growth inhibition (Fig. 10, g) is more consistent and

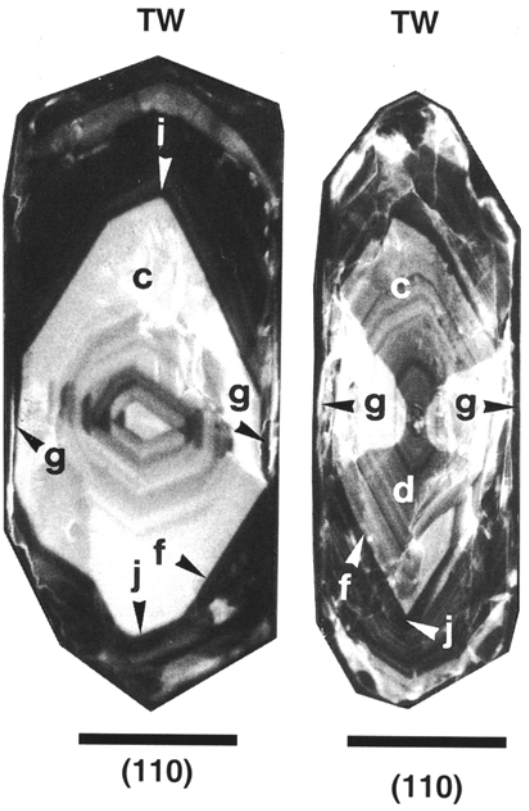

Fig. 10 Cathodoluminescence images of zircon sections from the autochthonous (anatectic) granodiorite in the Tauern window (sample *TW*). For lettering see Fig. 8

caused the disappearance of the {010} prism from the external shape of most crystals. It is not observed that {110} faces resumed growth, once they were inhibited. Also, there is no evidence that internal morphologies have been rounded by corrosion. A sharp transition to an outer low-luminescent and morphologically distinctive growth zone is present in most crystals (Fig. 10f). The behaviour of the {010} prism is not documented, because all crystals are sectioned parallel to the dominant (110) prism face. The general morphological evolution is summarized in Fig. 6.

Fig. 8 Cathodoluminescence images of zircon sections from the calcalkaline Budduso pluton (samples *BU1* to *BU4*). *a*, intermittent stages of crystal corrosion partly overgrown by brightly luminescent zones; *b*, minima of {010} growth rate; *c*, increasing growth rate of individual {011} faces causing enlargement of adjacent {121} pyramidal faces (the typical irregular shape of sector boundaries is marked by *dashed lines*; *d*, discontinuous growth bursts of {011}; *e*, gradual and systematic decrease of {010} growth rate (some smoothly curved sector boundaries are marked by *dashed lines*; *f*, discontinuous transitions to outer low-luminescent growth zones; g growth inhibition of {110}; *h*, resumption of rapid growth on inhibited {110} face, subsequent to a stage of corrosion; *i*, undisturbed growth of {010} in the outer low-luminescent zone; *j*, sharp transition from asymmetric and fast to symmetric and slow growth of {011}; *k*, sharp increase of {121} growth rate; *l*, inherited cores. *Scale bars* 30 μm. The indices below denote the section plane

Face-specific growth behaviour: theory and observations

In the following, the characteristic growth behaviour of the major crystal forms of zircon will be analysed and compared with predictions from crystal growth theory. The theoretical growth morphology of zircon, which is derived from the crystal structure alone, is predicted by the periodic bond chain (PBC) theory (Hartman 1987; Woensdregt 1992). Theoretical morphologies are usually not realized in natural growth environments, but they serve as a reference to evaluate the control from external factors. The theoretical morphology of zircon consists only of the crystal forms {010} and {011} (Fig. 11; Woensdregt 1992). Only these are predicted to grow by

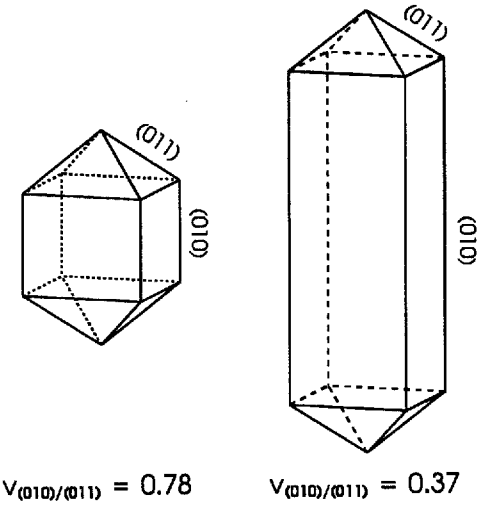

Fig. 11 Theoretical growth morphologies of zircon as predicted by the PBC-theory (Woensdregt 1992)

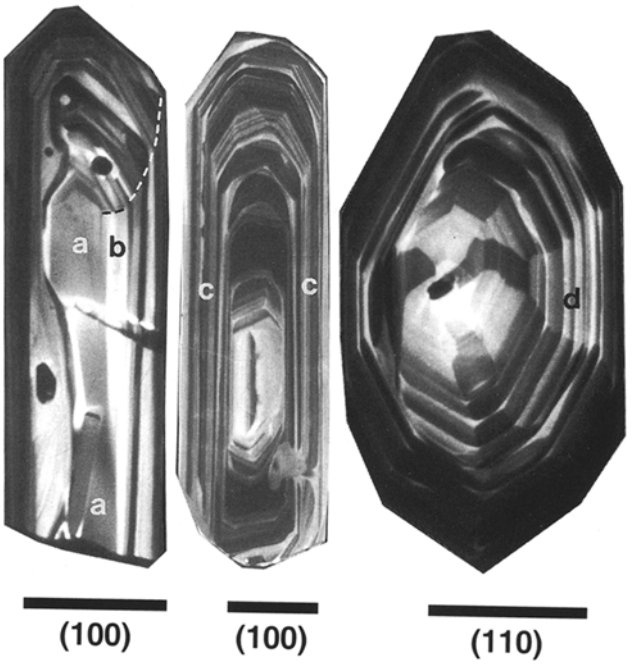

Fig. 12 Cathodoluminescence images of zircon sections showing the growth behaviour of prism faces. *a*, internal needle (dendritic) morphology; *b*, gradually decreasing growth rate of (010) relative to the pyramidal faces (the curved sector boundary is marked by a *dashed line*); *c*, low relative growth rate of (010) associated with intermittent periods of corrosion; *d*, rapid growth of (110) on corrosion stages. *Scale bars* 30 μm. The indices below denote the section planes

a layer mechanism (F-forms). The remaining forms classify as S-forms, implying growth by the faster adhesive mechanism. Due to their rapid growth, they are not present in the theoretical morphology.

{010} prism

The PBC-theory derives {010} as the F-form of zircon with the lowest growth rate (Fig. 11; Woensdregt 1992). It also predicts in a general way that, among several F-forms, those with lower growth rates in the theoretical morphology are more strongly accelerated by supersaturation (Hartman 1987; p 304). At increasing supersaturation, the growth rates of F-forms converge and the crystal habit tends to become equant as long as conditions for skeletal growth are not reached. The increase of the {010} growth rate relative to {011} by supersaturation is supported by observations. Crystals with a transition from acicular (dendritic) to polyhedral morphology (Fig. 12a) show a gradually decreasing relative growth rate of {010} during polyhedral growth (Fig. 12b). Evidently, supersaturation decreased after formation of the dendrite and the decreasing rate of {010} growth is the morphological response. At the opposite, conditions of very low supersaturation can be assumed for those growth intervals which are repeatedly interrupted by crystal corrosion (Fig. 12c). Here, the lowest growth rates of {010} relative to pyramidal faces are observed. The principal factor causing supersaturation in a crystallizing magma is the cooling rate, and it is concluded that this controls the relative growth rate of {010} most strongly.

{011} pyramid

{011} is the second F-form of zircon (Fig. 11). It is distinguished from {010} by the existence of more than one possible atomic structure of its crystal faces (Woensdregt 1992). The theory predicts that the adsorption of cations on the charged {011} faces changes the relative surface energies of the possible structures and that this changes the growth mechanism and growth rate. If adsorption makes the surface energies of two possible structures equal, growth can proceed by the attachment of half slices (thickness $d_{(022)}$), which is approximately twice as fast as the growth by whole elementary layers (thickness $d_{(011)}$). Figure 11 shows two theoretical morphologies corresponding to the alternative growth rates of {011}. The surface energies of several structures will not remain equal, if minor changes in the proportion of adsorbing cations occur. The theory reasonably explains the asymmetric, highly variable and unsteady growth of {011} (in the non-alkaline granitoids), but it does not predict which cations will preferentially adsorb on {011} and are responsible for the different growth behaviour in the alkaline and non-alkaline magmas.

{110} prism

According to the PBC-theory, {110} is an S-form and is not present in the theoretical growth morphology (Fig. 11). From the theoretical derivation of the atomic structure exposed at the {110} faces, Woensdregt (1992) concluded that the adsorption of protons may cause

{110} to acquire F-characteristics. He also considered that protons in the natural growth environment are provided by H_2O-molecules and hydrated complexes. The adsorption of these large and neutral molecules is likely to cause growth inhibition. Without experiments, it cannot be verified that H_2O controls the growth of {110} in a magma, but the observation that rapid growth can suddenly resume on inhibited {110} faces (Fig. 4, CD j, k; Fig. 8, BU3 h) strongly supports the suggestion that adsorption layers are responsible for the growth inhibition. A small amount of corrosion at the crystal surface is sufficient to disrupt the adsorption layer and allows crystal faces to return to high growth rates until the adsorption layer is rebuilt. Figure 12d shows that interspersed corrosion events keep the growth rate of {110} high.

Besides H_2O, other elements may also be present in the adsorption layer and cause growth inhibition. Benisek and Finger (1993) suggest that the low concentration of U and Th in the {110} sectors of zircon implies growth inhibition by these elements. This does not change the petrogenetic interpretation, because the enrichment of these elements in residual liquids parallels that of H_2O.

{121} and {031} pyramids

These pyramidal forms grew with a constant average rate which is slightly less than that of {011}. No peculiar growth behaviour (systematic tendencies, rapid fluctuations, growth inhibition), as discussed for the other crystal forms, is observed. The PBC-theory classifies both pyramids as S-forms (Woensdregt 1992). However, the observed behaviour is that of normal F-forms. Adsorption layers being permanently present in the magmatic environment may cause this discrepancy between theoretical and observed morphology.

Since the adjacent crystal forms ({011}, {010}, {110}) are more variable in growth rate, the sizes of {121} and {031} in the shape of crystals are principally controlled by geometrical relationships. Rapid growth of {010}, in the alkaline granitoids, favoured the presence and increasing size of {031}. The rapid growth intervals of {011} faces, in the calcalkaline and anatectic granitoids, increased the size of the adjacent {121} faces.

Discontinuous morphological evolution at late crystallization stages

The sharp morphological and chemical discontinuity (drop in cathodoluminescence) at late stages of zircon crystallization (observed in calcalkaline and anatectic granitoids) is difficult to explain by changing cooling rate (supersaturation) and chemical composition of the magma. Another environmental factor known to have a fundamental control on crystal morphology, is the formation of large growth units (from small ionic entities)

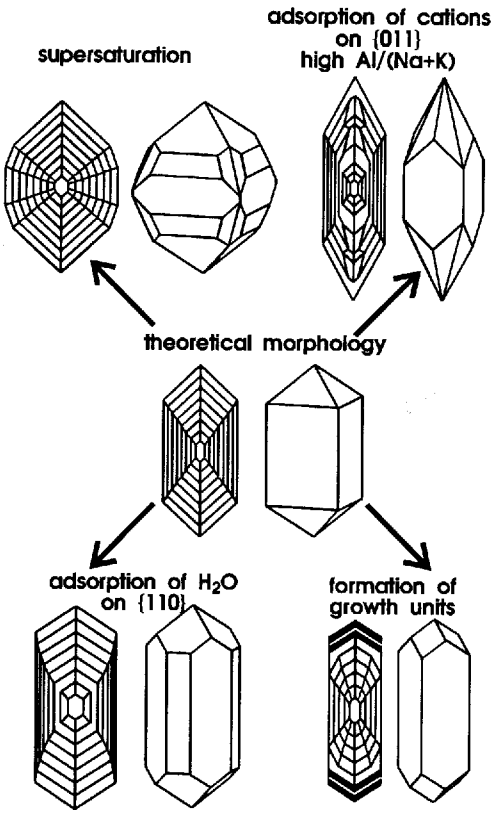

Fig. 13 Deviations from the theoretical growth morphology of zircon induced by environmental factors

in the liquid, before they are assembled on the crystal (Sunagawa 1984, p 91; Sunagawa 1987, p 537). Growth units can dramatically change the morphological evolution of crystals. The resulting morphology is not predicted by the theory, because the structure and size of the units are largely unknown. For zircon, a {110}- and {011}-dominated habit resulted from the discontinuous changes of relative growth rates described above. The formation of growth units starts when the magma attains sufficiently low temperatures and high concentrations of elements essential for the units. The observed drop in cathodoluminescence in zircon is known to be related to an increased concentration of impurity elements (U, Th, Y, P, REE; Sommerauer 1974). Probably, these elements are more readily incorporated in the zircon crystal, if they form part of growth units. This may explain the coincidence of the morphological and chemical discontinuity.

Figure 13 summarizes the deviations from the theoretical growth morphology of zircon caused by supersaturation, adsorption of cations on {011}, adsorption of H_2O or trace elements on {110}, and formation of growth units in the liquid.

Origin of different zircon morphologies in the sampled granitoid types

The observations show that the morphological evolution of zircon varies systematically between the different granitoid types. Although the number of samples studied in this way is low, the different morphologies are thought to reflect characteristic aspects in the evolution of alkaline, calcalkaline, and anatectic magmas. This assumption is justified by the previously established empirical relationship between external morphology and granitoid type (Pupin 1980) and by the correspondence between internal and external morphology observed in the present study.

The thermal history of a granitic magma primarily determines the supersaturation and, thus, controls the relative growth rate of {010}. Zircons from the alkaline granites crystallized, for their major part, during a period with a constant and rather high cooling rate of the magma. This caused the permanently high growth rate of {010} relative to the pyramids. The long and uninterrupted cooling history may result from the ascent of the magma from the lower crust. The strongly reduced growth rate of {010}, at late stages, indicates that the cooling rate dropped sharply. This may be related to the storage of the magma in a chamber, before it was finally injected into the volcanic edifice. Some corrosion of zircon occurred in the magma chamber, possibly caused by renewed influx of fresh and hot magma. A final high cooling rate must be assumed for magmas injected as dykes, but this is not recorded in the zircon morphology. Probably, too little material was added on the already existing large crystal faces during the short injection event.

In the calcalkaline magmas, the thermal history was more variable. Zircon growth was, from the beginning and repeatedly, interrupted by periods of low supersaturation and crystal corrosion. In the zoned pluton of Budduso this evolution corresponds to magma mixing. Towards the centre of the pluton, evidence for magma mixing decreases and the thermal history becomes uniform. The gradual reduction of the relative growth rate of {010} indicates that the cooling rate of the magma decreased continuously. This is the thermal evolution expected for a pluton which crystallizes in-situ after its final emplacement.

The chemistry of the magma is the main control on the growth of the adsorption-sensitive {011} pyramid. From the chemical analyses (Table 1), it is possible to establish rough empirical relationships between cation ratios in the magma and the growth behaviour of {011}. Considering the major elements, a high agpaicity index (alkaline magmas) is apparently related to slow and symmetric growth of {011}, whereas a low agpaicity index (calcalkaline and anatectic magmas) is apparently related to fast and asymmetric growth of {011}. Since the growth rate of {011} determines the size of adjacent {121}, the relative sizes of {011} and {121} appear to be related to agpaicity, in agreement with the empirical findings of Pupin (1980). However, agpaicity is only one possible factor, and other elements (Ca, trace elements) may have resulted in variable growth of {011}. Magma chemistry does not control the growth rate of {011} directly. Rather, it is the adsorption layer of cations on the {011} faces, which determines the growth mechanism and rate. Corrosion events at the crystal faces may disturb or destroy the adsorption layers and cause changes in the growth rate of {011} faces, which are not related to a changing magma chemistry. This happened at the late stages of zircon crystallization in the alkaline magmas, where {011} started to grow asymmetrically after stages of corrosion.

The effect of H_2O on zircon morphology, as predicted by the theory, is consistent with the observed relationship between the growth of {110} and the geological and petrographic characteristics of the samples. In the alkaline granitoids, with an anhydrous mineral paragenesis and with no crustal contamination, {110} is absent, as in the theoretical morphology. It is ubiquitously present as an F-form in the calcalkaline and anatectic granitoids, which all have a hydrous mineral assemblage. In the zoned pluton, the transition from amphibole- to biotite-carrying parageneses towards the centre of the pluton (Fig. 3) indicates an increasing concentration of H_2O in the magma. Accordingly, the tendency of {110} faces to become growth-inhibited at late stages of crystallization is strongest in the centre of the pluton. In all calcalkaline samples resumption of rapid growth on some inhibited {110} faces is observed. This happened after corrosion events which disrupted the adsorption layers and which are likely to be related to magma mixing. The biotite-rich authochthonous granodiorite shows the strongest tendency of {110} faces towards growth inhibition. In the absence of magma mixing, corrosion of crystals did not occur. Therefore, the adsorption layers remained in place and did not allow for resumption of growth on inhibited faces.

The formation of growth units in the liquid causing the observed discontinuities in the morphological evolution of zircon can start at some stage of magma differentiation, most likely in the residual liquid which reaches the highest concentration of incompatible elements. The morphological discontinuities within zircon are observed in those granitoids (anatectic granodiorite, calcalkaline pluton), which were autochthonous or emplaced at a rather deep level. The final cooling rate of these magmas was low and crystallization from the residual liquid may have occurred over an extended period of time.

Conclusions

This study supports and extends the empirical relationship between zircon morphology and type of granitic rock. The external crystal shape, on which previous studies are based, is just the final stage of a much more diversified internal morphology. For the first time, the

morphological evolution of zircon from several granitic rocks is presented in a partly quantitative way. Sharp, discontinuous and erratic changes in the growth rates of crystal faces are more important for the evolving morphology than gradual and systematic changes. This observation contradicts the previous understanding that zircon morphology evolves continuously in response to changing temperature and chemistry of the magma. Most of the variation of relative growth rates of crystal faces is due to the formation and destruction of adsorption layers. The relative proportion of the pyramidal forms {010} and {110} is dominantly controlled by the growth inhibition of {110} due to adsorption of components (probably H_2O) enriched in the residual liquid of the calcalkaline and anatectic magmas. An effect of temperature on the pyramidal ratio must be excluded. Growth inhibition of {110} is also responsible for the strongly increasing elongation of zircon crystals in H_2O-enriched residual magmas. The pyramidal evolution of zircon results mainly from the variable growth rate of {011}. It is controlled by the chemistry of the magma (agpaicity), but a simple dependence on changing element concentrations is ruled out by the irregular and asymmetric growth of {011}. The only crystal form for which gradual and systematic changes of growth rates are observed is the {010} prism. Its constant and high growth rate during magma ascent (alkaline magma) and the systematically decreasing growth rate after emplacement (calcalkaline magma) are consistent with a dependence on the cooling rate.

The final trend towards {110}- and {011}-dominated crystal shapes in the calcalkaline and anatectic granitoids is due to the presence of a discontinuity in the morphological evolution. The only reasonable explanation is the formation of growth units in the residual liquid.

Acknowledgements This work was supported by the Schweizerischer Nationalfonds zur Förderung der wissenschaftlichen Forschung (21-31069.91), which is greatfully acknowledged. The critical comments of W. Hansmann substantially improved an earlier version of the manuscript. I am further indebted to J. Hanchar, F. Oberli, D. Gebauer, C.F. Woensdregt and an anonymous reviewer for constructive comments and discussions. S. Barth kindly provided the zircon sample from the Cima d'Asta pluton. The cathodoluminescence imaging was carried out at the Department of Metallurgical Sciences (ETH Zürich). Crystals and sections were drawn by the program SHAPE (copyright 1992 by E. Dowty, Shape Software).

References

Barth S, Oberli F, Meier M, Blattner P, Bargossi M, di Battistini G (1993) The evolution of a calc-alkaline basic to silicic magma system:geochemical and Rb-Sr, Sm-Nd, and $^{18}O/^{16}O$ isotopic evidence from the Late Hercynian Atesina-Cima d'Asta volcano-plutonic complex, northern Italy. Geochim Cosmochim Acta 57:4285–4300

Barth S, Oberli F, Meier M (1994) Geochronology in the southern Alps (N Italy): allanite Th-Pb dating of rhyolite and granodiorite from the Late Hercynian Atesina-Cima d'Asta volcano-plutonic complex. Earth Planet Sci Let (in press)

Benisek A, Finger F (1993) Which factors control the prism tracht of granite zircons. Contrib Mineral Petrol 114:441–451

Bonin B (1977) Les complexes granitiques subvolcaniques de Corse: caractéristiques, signification et origine. Bull Soc Géol Fr 7:865–871

Bonin B (1988) Peralkaline granites in Corsica:some petrological and geochemical constraints. Rend Soc Ital Mineral Petrol 43:281–306

Bonin B, Grelou-Orsini C, Vialette Y (1978) Age, origin and evolution of the anorogenic complex of Evisa (Corsica): a K-Li-Rb-Sr study. Contrib Mineral Petrol 65:425–432

Bonin B, Platevoet B, Vialette Y (1987) The geodynamic significance of alkaline magmatism in the western Mediterranean compared with West Africa. Geol J 22:361–387

Bruneton P, Orsini JB (1977) Le massif granitique de Budduso (Sardaigne nord-orientale): une seule intrusion de type zone concentrique. C R Acad Sci Sér D 284:151–154

Caruba R (1978) Morphologie de zircons synthétiques: corrélations pétrogénétiques. Can Mineral 16:315–323

Caruba R, Baumer A, Hartman P (1988) Crystal growth of synthetic zircon round natural seeds. J Crys Growth 88:297–302

Cliff RA (1981) Pre-Alpine history of the Pennine zone in the Tauern window, Austria: U-Pb and Rb-Sr geochronology. Contrib Mineral Petrol 77:262–266

Cocirta C, Orsini JB, Coulon C (1989) Exemples de mélange de magmas en contexte plutonique: les enclaves des tonalites-granodiorites du massif de Bono (Sardaigne septentrionale). Can J Earth Sci 26:1264–1281

d'Amico C, Franceschini C (1985) An example of H_2O-undersaturated granitic magma: a case study of partially-melted aplite xenoliths in granite porphyries from the Cima d'Asta intrusive complex, southern Alps, Italy. Mineral Petrogr Acta 29:139–144

Finger F, Steyrer HP (1988) Granite-types in the Hohe Tauern (Eastern Alps, Austria) – some aspects on their correlation to Variscan plate tectonic processes. Geodinamica Acta 2:75–87

Finger F, Frasl G, Haunschmid B, Lettner H, von Quadt A, Schermaier A, Schindlmaier AO, Steyrer HP (1993) The Zentralgneise of the Tauern Window (Eastern Alps) – insight into an intra-Alpine Variscan batholith. In: von Raumer JF, Neubauer F (eds) Pre-Mesozoic geology in the Alps. Springer, Berlin Heidelberg New York, pp 375–391

Frisch W, Vavra G, Winkler M (1993) Evolution of the Penninic basement of the Eastern Alps. In: von Raumer JF, Neubauer F (eds) Pre-Mesozoic geology in the Alps. Springer, Berlin Heidelberg New York, pp 349–360

Hartman P (1987) Modern PBC theory. In: Sunagawa I (ed) Morphology of crystals. Terra Scientific, Tokyo, pp 269–319

Holub B, Marschallinger R (1989) Die Zentralgneise im Hochalm-Ankogel-Massiv (östliches Tauernfenster). Teil I: petrographische Gliederung und Intrusionsfolge. Mitt Österr Geol Ges 81:5–31

Karner FR, Helgesen JO (1970) Petrologic significance of zircon variation in the Tunk Lake Granite, southeastern Maine. J Geology 78:480–498

Köhler H (1970) Die Änderung der Zirkonmorphologie mit dem Differentiationsgrad eines Granits. N Jahrb Mineral Monatsh (9)405–420

Paterson BA, Stephens WE, Rogers G, Williams IS, Hinton RW, Herd DA (1992) The nature of zircon inheritance in 2 granite plutons. Trans R Soc Edinburgh: Earth Sci 83:459–471

Poldervaart A (1956) Zircon in rocks:2. Igneous rocks. Am J Sci 254:521–554

Pupin JP (1980) Zircon and granite petrology. Contrib Mineral Petrol 73:207–220

Pupin JP, Turco G (1972) Une typologie originale du zircon accessoire. Bull Soc Fr Minéral Cristallogr 95:348–359

Pupin JP, Turco G (1975) Typologie du zircon accessoire dans les roches plutoniques dioritiques, granitiques et syentiques. Facteurs essentiels déterminant les variations typologiques. Pétrologie 1:139–156

Pupin JP, Turco G (1981) Le zircon, minéral commun significatif des roches endogènes et exogènes. Bull Minéral 104:724–731
Shelley D (1993) Igneous and metamorphic rocks under the microscope. Chapman and Hall, London
Sommerauer J (1974) Trace element distribution patterns and the mineralogical stability of zircon – an application for combined electron microprobe techniques. Proc Electron Microscopy Society of Southern Africa 4:71–72
Speer JA (1982) Zircon. In: Ribbe PH (ed) Orthosilicates, 2nd edn (Reviews in Mineralogy, vol 5). Mineralogical Society of America, Washington DC, pp 67–112
Sunagawa I (1984) Growth of crystals in nature. In: Sunagawa I (ed) Materials science of the Earth's interior. Terra Scientific, Tokyo, pp 63–105
Sunagawa I (1987) Morphology of minerals. In: Sunagawa I (ed) Morphology of crystals. Terra Scientific, Tokyo, pp 511–587
Vavra G (1989) Die Entwicklung des penninischen Grundgebirges im östlichen und zentralen Tauernfenster der Ostalpen – Geochemie, Zirkonmorphologie, U/Pb-Radiometrie. Tübinger Geowiss Abh Reihe A 6, pp 150
Vavra G (1990) On the kinematics of zircon growth and its petrogenetic significance: a cathodoluminescence study. Contrib Mineral Petrol 106:90–99
Vavra G (1993) A guide to quantitative morphology of accessory zircon. In: Watson EB, Harrison TM, Miller CF, Ryerson FJ (ed) Geochemistry of accessory minerals. Chem Geol 110: 15–28
Vavra G and Hansen BT (1991) Cathodoluminescence studies and U/Pb dating of zircons in pre-Mesozoic gneisses of the Tauern Window – implications for the Penninic basement evolution. Geol Rundsch 80:703–715
Veniale F, Pigorini B, Soggetti F (1968) Petrological significance of accessory zircon in the granites from Baveno, M. Orfano and Alzo (North Italy). Proc 23rd Int Geol Congr 13:243–268
Woensdregt CF (1992) Computation of surface energies in an electrostatic point charge model:II. Application to zircon. Phys Chem Mineral 19:59–69
Zorpi MJ, Coulon C, Orsini JB, Cocirta C (1989) Magma mingling, zoning and emplacement in calc-alkaline granitoid plutons. Tectonophysics 157:315–329